JOURNAL OF GEOPHYSICAL RESEARCH, VOL. 108, NO. D24, 4798, doi:10.1029/2003JD003812, 2003

Twentieth-century temperature and precipitation trends in ensemble climate simulations including natural and anthropogenic forcing

Anthony J. Broccoli,[1] Keith W. Dixon, Thomas L. Delworth, Thomas R. Knutson, and Ronald J. Stouffer
NOAA/Geophysical Fluid Dynamics Laboratory, Princeton University, Princeton, New Jersey, USA

Fanrong Zeng
RSIS, Princeton, New Jersey, USA

Received 28 May 2003; revised 19 September 2003; accepted 10 October 2003; published 31 December 2003.

[1] We present results from a series of ensemble integrations of a global coupled atmosphere-ocean model for the period 1865–1997. Each ensemble consists of three integrations initialized from different points in a long-running GFDL R30 coupled model control simulation. The first ensemble includes time-varying forcing from greenhouse gases only. In the remaining three ensembles, forcings from anthropogenic sulfate aerosols, solar variability, and volcanic aerosols in the stratosphere are added progressively, such that the fourth ensemble uses all four of these forcings. The effects of anthropogenic sulfate aerosols are represented by changes in surface albedo, and the effects of volcanic aerosols are represented by latitude-dependent perturbations in incident solar radiation. Comparisons with observations reveal that the addition of the natural forcings (solar and volcanic) improves the simulation of global multidecadal trends in temperature, precipitation, and ocean heat content. Solar and volcanic forcings are important contributors to early twentieth century warming. Volcanic forcing reduces the warming simulated for the late twentieth century. Interdecadal variations in global mean surface air temperature from the ensemble of experiments with all four forcings are very similar to observed variations during most of the twentieth century. The improved agreement of simulated and observed temperature trends when natural climate forcings are included supports the climatic importance of variations in radiative forcing during the twentieth century. *INDEX TERMS:* 1620 Global Change: Climate dynamics (3309); 3309 Meteorology and Atmospheric Dynamics: Climatology (1620); 3337 Meteorology and Atmospheric Dynamics: Numerical modeling and data assimilation; *KEYWORDS:* climate modeling, global change

Citation: Broccoli, A. J., K. W. Dixon, T. L. Delworth, T. R. Knutson, R. J. Stouffer, and F. Zeng, Twentieth-century temperature and precipitation trends in ensemble climate simulations including natural and anthropogenic forcing, *J. Geophys. Res.*, *108*(D24), 4798, doi:10.1029/2003JD003812, 2003.

1. Introduction

[2] A key aspect of understanding the changes in climate during the last century is to determine the role of time-dependent radiative forcing. There is very strong evidence that such forcing has occurred during this time period, with both natural and anthropogenic changes in the radiative environment contributing to the forcing. Some of the radiative changes, such as the variations in radiatively active trace gases, are well-constrained by direct and indirect measurements. The rest are known only with substantial uncertainties, primarily because of a combination of inadequate measurements and incomplete understanding of their radiative effects. Nevertheless, the available evidence suggests that each of these forcings has the potential to influence the time-dependent behavior of global climate during the period of instrumental observations [*Ramaswamy et al.*, 2001].

[3] The potential importance of future changes in climate has placed much of the focus on the effects of the large changes in radiative forcing projected to occur in response to continuing anthropogenic emissions of greenhouse gases. A retrospective analysis of climate change requires a somewhat different focus, since the magnitude of natural radiative forcing is comparable to the human-induced component of radiative forcing during a good portion of the last century. More than twenty years ago, *Hansen et al.* [1981] noted that volcanic and solar effects may have been the major causes of fluctuations about the overall warming

[1]Now at Department of Environmental Sciences, Rutgers University, New Brunswick, New Jersey, USA.

0148-0227/03/2003JD003812$09.00

trend during the period of instrumental climate observations. More recently, an increased recognition of the importance of natural forcings is evident in the Third Assessment Report of the Intergovenmental Panel on Climate Change (IPCC TAR [*Houghton et al.*, 2001]) and is derived, at least in part, from studies that attribute some of the observed changes in climate to natural forcings [*Tett et al.*, 1999; *Crowley*, 2000; *Stott et al.*, 2000, 2001; *Meehl et al.*, 2003].

[4] This study explores this topic further by using a coupled atmosphere-ocean model to evaluate the contributions of anthropogenic and natural forcings to trends in temperature and precipitation during the twentieth century. The forcings employed are those due to increasing greenhouse gas concentrations, the effects of tropospheric sulfate aerosols, variations in total solar irradiance, and the effects of volcanic aerosols in the stratosphere. Because the internal variability of the climate system may also be imprinted on the climate record, the impact of such variability is estimated by running ensembles in which each member has a different initial condition. The results from four different ensembles, each of which uses a different combination of forcings, also allow us to assess the degree of realism with which the climate model can simulate multidecadal to centennial trends in surface climate. Confidence in projections of future trends in climate depends, in part, on the successful simulation of such trends.

2. Model Description

[5] The model used in this study consists of coupled general circulation models of the atmosphere and the ocean, with land surface and sea ice components also included. This model is identified as GFDL_R30_c in the nomenclature of the IPCC TAR [*Cubasch et al.*, 2001, Table 9.1]. The GFDL_R30_c model is similar to earlier versions of GFDL coupled models [e.g., *Manabe et al.*, 1991], but with enhanced horizontal and vertical resolution. The description of the model is this section is brief and intended to emphasize the basic characteristics of the model, and the reader should refer to *Delworth et al.* [2002] for a more complete description.

[6] The atmospheric component employs the spectral transform method with rhomboidal truncation at zonal wave number 30, corresponding to a transform grid spacing of approximately 2.2° latitude by 3.75° longitude. Fourteen unevenly spaced sigma coordinate levels are used for vertical differencing. Insolation at the top of the atmosphere varies seasonally, but not diurnally, and clouds are predicted whenever the relative humidity exceeds a critical threshold. The land surface model features prognostic snow cover and soil moisture based on a simple "bucket" model. Surface temperature is determined diagnostically, based on the assumption that there is no heat stored in the soil.

[7] The ocean component of the coupled model is based on version 1.1 of the Modular Ocean Model [*Pacanowski et al.*, 1991], which solves the primitive equations of motion using the Boussinesq, rigid-lid and hydrostatic approximations. The horizontal grid spacing is 2.25° latitude by 1.875° longitude, with depth as the vertical coordinate and 18 unevenly spaced levels. Sea ice is simulated by a simple thermodynamic model, in which ice is treated as a single layer with no sensible heat content. Sea ice is advected by ocean currents, but additional convergence is not permitted once the sea ice thickness exceeds a critical value. The formation of leads is not included.

[8] The atmospheric and oceanic components of the model exchange fluxes of heat, water and momentum once a day. The heat flux consists of the radiative, sensible and latent components, and the water flux includes evaporation, sublimation, precipitation and runoff from the continents. In addition to these physical fluxes, so-called "flux adjustment" terms for heat and water are added to the ocean component to compensate for the mismatch between the fluxes needed by each component to maintain a realistic climate. The flux adjustments are determined prior to the start of the coupled model integration. They vary seasonally and spatially, but do not vary from one year to the next. Because the flux adjustments are independent of the state of the coupled model, they do not systematically damp or amplify anomalies of sea surface temperature or sea surface salinity. The use of flux adjustments is successful in greatly limiting the long-term drift of the model [*Manabe et al.*, 1991].

3. Experimental Design

[9] Time-dependent radiative forcings from changes in greenhouse gases, tropospheric sulfate aerosols, solar irradiance and stratospheric volcanic aerosols are imposed in a series of coupled model integrations covering the period from 1865 to 1997. The forcings are applied sequentially in an effort to minimize the total computational requirements while using preexisting model runs that had been made for other purposes. To improve the chances of extracting the signals of climate change from the noise of the model's internal variability, an ensemble consisting of three separate integrations is run for each combination of forcings.

3.1. G Ensemble

[10] The G ensemble includes only the radiative forcing from increasing greenhouse gases, including carbon dioxide, methane, nitrous oxide, and chlorofluorocarbons. The combined effects of these gases is represented as a change in carbon dioxide with an equivalent radiative forcing [e. g., *Mitchell and Johns*, 1997]. The time dependence of the radiative forcing is taken from *Shine et al.* [1990], with the extension beyond 1990 to 1997 according to the IS92a scenario of the IPCC [*Leggett et al.*, 1992]. The time series of radiative forcing (relative to the preindustrial atmosphere) for the G ensemble (Figure 1a, red curve) features a slow rise from a value of $\sim$0.4 W m^{-2} in 1865 to $\sim$1.2 W m^{-2} in 1960. A more rapid rise follows thereafter, with the radiative forcing approaching 3 W m^{-2} by 1997.

[11] The nonzero radiative forcing in 1865 implies that greenhouse gas concentrations had risen above preindustrial levels before that date. To reduce the length of our experiments, we did not include this gradual increase in forcing in the G ensemble or any of our other model runs. Instead, the greenhouse gas concentrations were instantaneously increased to 1865 levels at the start of each of the integrations. This can lead to the "cold start" phenomenon, in which the simulated climate is systematically colder than it would have been had the increase in forcing been applied at its actual rate [*Hasselmann et al.*, 1993]. The cold start is due to the

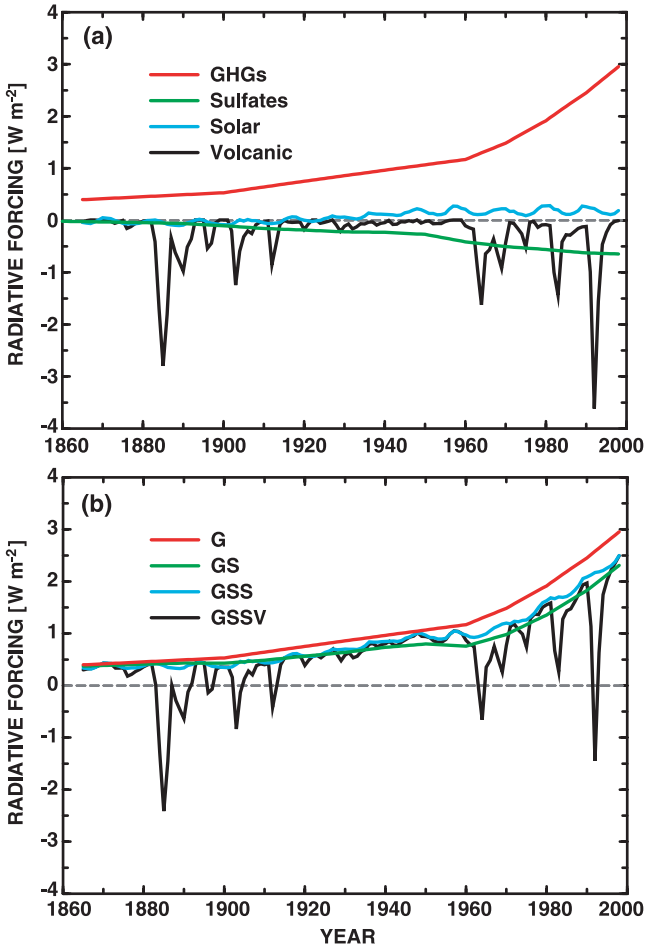

Figure 1. (a) Temporal variation in radiative forcing (W m^{-2}) relative to preindustrial conditions resulting from variations in greenhouse gases (red), tropospheric sulfate aerosols (green), solar irradiance (green) and volcanic aerosols (black). (b) Temporal variations in total radiative forcing (W m^{-2}) relative to preindustrial conditions for the G (red), GS (green), GSS (blue) and GSSV (black) ensembles.

thermal inertia of the ocean, which delays the response of the climate system to time-dependent changes in forcing. Because our analysis of these experiments will focus on changes in climate during the twentieth century, the cold start should not adversely influence our results, as *Dixon and Lanzante* [1999] have shown its effects to diminish in the decade or two after the start of an integration.

3.2. GS Ensemble

[12] The GS ensemble includes greenhouse gas forcing from the G ensemble plus the direct radiative effects of tropospheric sulfate aerosols resulting from human activities. Indirect effects associated with potential aerosol-induced changes in cloud albedo are not included. Sulfate aerosols are not directly treated by the coupled model's radiation code; instead, their radiative effects are represented as a perturbation of the surface albedo [*Mitchell et al.*, 1995; *Mitchell and Johns*, 1997; *Haywood et al.*, 1997]. The assumed radiative properties of sulfate aerosols and the procedure follows *Haywood et al.* [1997], with the albedo perturbations recalibrated for the climate of the GFDL_R30_c model. As in the studies cited previously, the present-day spatial pattern of sulfate aerosol loading comes from the sulfur cycle model of *Langner and Rodhe* [1991]. Spatial patterns for earlier years are obtained by scaling this pattern by the time series of global mean industrial sulfate emissions. This procedure is described in greater detail by *Mitchell and Johns* [1997].

[13] The time series of tropospheric aerosol forcing (Figure 1a, green curve) is negative throughout the period of integration, consistent with the dominance of the scattering effects of sulfate aerosols. The forcing is quite small through the early part of the twentieth century, but its magnitude increases more rapidly between 1950 and 1970. Some slowing of the increase in magnitude is evident during the last few decades, with tropospheric aerosol forcing reaching -0.7 W m^{-2} by 1997.

[14] Because tropospheric aerosol forcing partially offsets greenhouse gas forcing, the radiative forcing in the GS ensemble (Figure 1b, green curve) is smaller than in the G ensemble. The G and GS ensembles are qualitatively similar in their time-dependence, although there is more of a plateau in forcing around 1960 in the GS ensemble. The total forcing in the GS ensemble increases to $\sim$2.4 W m^{-2} by the end of the last century.

3.3. GSS Ensemble

[15] The GSS ensemble adds the radiative forcing originating from variations in total solar irradiance to the anthropogenic forcings included in the GS ensemble. Because accurate observations of total solar irradiance are limited to the satellite era, a reconstructed solar irradiance time series must be used for much of the period of integration. We use the solar irradiance time series of *Lean* [2000], which blends satellite observations for the recent period with a reconstruction based on astronomical observations of sunspot numbers for the presatellite era. The solar irradiance time series contains a high-frequency component related to the 11-year sunspot cycle, and a low-frequency component, which is determined from low-frequency variations in annual sunspot group numbers. Although the observed changes in solar irradiance are larger in the ultraviolet portion of the solar spectrum, the forcing for the coupled model is assumed to be independent of wavelength. We do not consider the indirect radiative effects that result from irradiance-induced variations in ozone concentration, although these may not be negligible [*Haigh*, 1996; *Shindell et al.*, 1999].

[16] The low-frequency solar forcing applied in the GSS ensemble (Figure 1a, blue curve) can be characterized by its behavior during three multidecadal periods. From the start of the integration period through the 1890s, there is a decrease to approximately -0.1 W m^{-2}. Solar irradiance then rises more sharply during the first half of the twentieth century, such that the forcing reaches +0.2 W m^{-2} by the 1940s. The latter half of that century features no important multidecadal trend, with only the 11-year solar cycle variations evident. When combined with the previously described forcings, the total forcing for the GSS ensemble (Figure 1b, blue curve) generally resembles that of GS ensemble in its long-term trends. The upward trend in solar irradiance during the early twentieth century adds to the combined effects of greenhouse gases and aerosols to yield a more rapid increase in

forcing during this period, as evident from the systematic shift of the GSS curve from below the GS curve near 1900 to above the GS curve after 1950.

3.4. GSSV Ensemble

[17] Volcanic eruptions that eject sulfur-rich material into the stratosphere can also be a source of radiative forcing of climate [e.g., *Robock*, 2000], and we include the effects of this forcing, as well as the other GSS ensemble forcings, in the GSSV ensemble. The volcanic forcing is taken from *Andronova et al.* [1999], which provides an estimate of the latitude- and time-dependent radiative forcing at the tropopause based on measurements of volcanic aerosols for recent years (i.e., after the eruption of Mt. Pinatubo in 1991) and estimates of aerosol optical depths for earlier periods. Because of the simplicity of the radiative transfer component of our coupled model, volcanic forcing is represented by latitude-dependent perturbations in incident solar radiation, calibrated to produce a spatiotemporal pattern of radiative forcing equivalent to the estimates by *Andronova et al.* [1999].

[18] The use of perturbations in incoming solar radiation as a surrogate for volcanic forcing is adequate for our purposes because this paper focuses on changes in annual mean climate at the earth's surface. *Hansen et al.* [2002] have shown that volcanic forcing and changes in solar irradiance induce very similar spatial patterns of surface air temperature response. Our methodology would not be adequate for studying the response of the stratosphere to volcanic forcing, since aerosol heating due to the absorption of solar and infrared radiation is important in that layer. Similarly, this methodology is inadequate for examining vertical variations in temperature trends, nor would it be appropriate for investigating the "winter warming" of high latitude continents following major volcanic eruptions, since this near-surface warming is postulated to occur in response to the downward propagation of circulation anomalies from the stratosphere [*Robock*, 2000].

[19] The time series of volcanic forcing (Figure 1a, black curve) shows a series of large negative excursions following each major aerosol-producing eruption, including Krakatau (1883), Santa Maria (1902), Agung (1963), El Chichón (1982) and Pinatubo (1991). These eruptions produce annual mean radiative forcing values from -1 to -4 W m^{-2}, with a subdecadal decay timescale. Volcanic forcing events primarily occurred during two periods, one from 1880–1915 and the other during the last four decades of the twentieth century. The episodic volcanic forcing, when averaged over this latter period, amounts to approximately -0.5 W m^{-2}. The addition of volcanic forcing makes the time series of total forcing in the GSSV ensemble (Figure 1b, black line) appreciably smaller than that of the GSS ensemble during each of the aforementioned periods.

3.5. Initialization of Model Integrations

[20] Each ensemble consists of three integrations, with initial conditions chosen from a control run of the GFDL_R30_c coupled model in which there are no interannual variations in forcing. *Delworth et al.* [2002] describe the method used to initialize the control run, and *Stouffer and Dixon* [1998] provide a more general discussion of coupled model initialization. The initial conditions are separated by at least 40 years, which leads to substantially different climate states because of the internal variability simulated in the control integration. The availability of different ensemble members with the same forcing allows us to make more robust estimates of the model's forced response, and the variability internal to an ensemble provides an estimate of the uncertainty associated with a single realization of forced climate response.

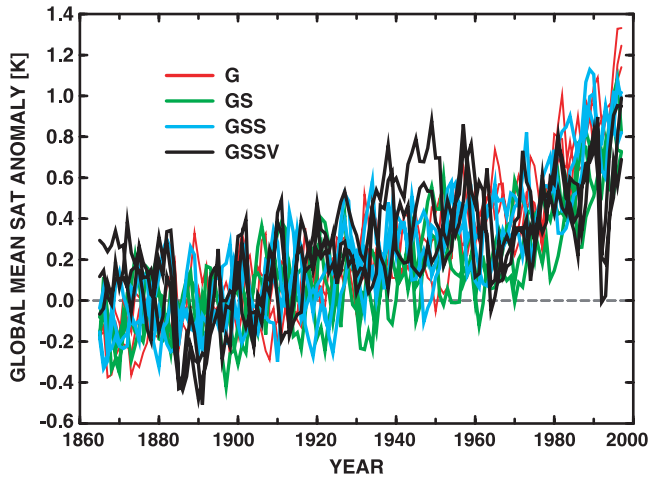

Figure 2. Temporal variation of annually averaged global mean surface air temperature anomalies for each member of the G (red), GS (green), GSS (blue) and GSSV (black) ensembles. Anomalies are created by subtracting the mean of the period 1880–1920.

4. Temperature Trends

[21] Time series of annually averaged global mean temperature are computed from each of the three members of the G, GS, GSS and GSSV ensembles. One could represent these twelve time series as anomalies with respect to the control run, in which case the time series could be regarded as simulated departures from the preindustrial climate. This method of standardization is inconvenient for comparisons with observations, however, due to the lack of widespread instrumental records of the preindustrial climate. Instead, we choose to express each global temperature time series as the departure from its mean over the period 1880–1920. This period is chosen because there is adequate data coverage to produce a reasonably good estimate of the observed global mean temperature, yet the period is early enough for differences in warming rates among the four ensembles to be visually evident at the end of the integrations. One consequence of this method of determining anomalies is that the relative coolness or warmth of each run relative to the others cannot be discerned, as each run can have a different mean temperature during the base period. Expressing the simulated global mean temperatures as anomalies from a particular base period does not have any impact on the calculation of linear temperature trends, which is the primary focus of this section.

[22] When plotted as anomalies from the 1880–1920 base period, the twelve time series exhibit a general upward trend (Figure 2), as might be expected considering the

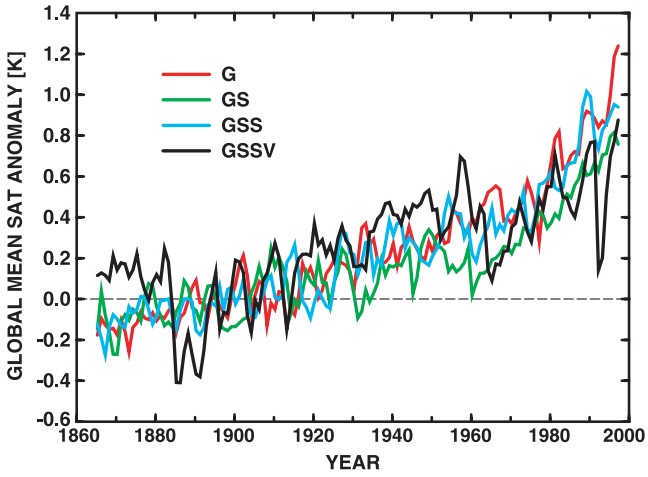

Figure 3. Same as Figure 2 except for ensemble means.

increasing radiative forcing over the course of all four forcing scenarios. Although there is considerable high-frequency variability, some systematic interensemble differences are evident from a visual inspection of the time series plots. There is a clear tendency for runs from the G ensemble (red curves) to emerge above the cluster of curves in the last two decades of the integration, and the GSSV runs (black curves) are distinguished by lower anomaly values during the same period. Other differences are more subtle, particularly with regard to trends during the early twentieth century.

[23] Averaging the time series belonging to each ensemble (Figure 3) eliminates some of the high-frequency variability, but with only three integrations per ensemble, the time series remain somewhat noisy, despite the relatively smooth forcing in all but the GSSV ensemble. For the full length of the integration, one can visually discern that the overall degree of warming is qualitatively in proportion to the change in radiative forcing over that period, being largest for the G ensemble and smallest for the GSSV ensemble.

[24] To examine more quantitatively the differences in warming rates, temperature trends are computed using a least squares linear fit. To avoid any distortions resulting from the cold start problem, trends are computed for three periods after 1900. The period from 1900–1997 is used to estimate centennial trends. To focus on the early twentieth century warming, which occurred during a time when increases in greenhouse gas forcing were relatively slow, trends for the period 1900–1940 are computed. Finally, the period from 1940–1997 is used to assess changes in temperature since the period of observed warmth centered around 1940. (Although shorter periods, such as the period of warming from 1970–1997, are also interesting, trends for such periods were found to differ so markedly among members of the same ensemble that they have not been presented.) For comparison, we use the same method to compute observed trends, using the merged land and ocean temperature data set developed in the Climatic Research Unit (CRU) of the University of East Anglia [*Jones et al.*, 1999], as well as the temperature data set developed at the Goddard Institute for Space Studies (GISS) from weather station records [*Hansen et al.*, 1999]. Differences in trends between the CRU and GISS data sets provide some measure of observational uncertainty.

[25] The ensemble mean temperature trend for each forcing scenario (Figure 4) and the range of trends from the individual members of each ensemble are computed. For the "full century" period, the spread of the ensemble members is quite small, amounting to less than 0.1 K $(100\ \mathrm{yr})^{-1}$. The largest ensemble mean temperature trend occurs with the G scenario. Addition of the sulfate forcing reduces the magnitude of the trend in the GS ensemble, and this sulfate cooling is nearly offset by the inclusion of solar irradiance in the GSS ensemble. The GSSV ensemble yields the smallest trend of 0.50 K $(100\ \mathrm{yr})^{-1}$.

[26] Assessing the consistency of simulated and observed trends is complicated by the uncertainty of observational estimates and the presence of internal variability in the climate system. We attempt to address the issue of observational uncertainty by using two temperature data sets. To account for internal variability, the simulated and observed trends are regarded as consistent if the range of ensemble members contains one or more of the observational estimates. By this definition, the GS and GSSV ensembles both yield temperature trends for the 1900–1997 period that are consistent with the observed estimates of 0.55 and 0.63 K $(100\ \mathrm{yr})^{-1}$ for the GISS and CRU data sets, respectively.

[27] During the period from 1900 to 1940, the observed global warming rate was somewhat larger than over the century as a whole, with observed estimates of 0.92 K $(100\ \mathrm{yr})^{-1}$ from both the CRU and GISS data sets (Figure 4). The simulated temperature trends for this early century period exhibit considerably more scatter than for the longer period, with intraensemble ranges of 0.4–0.8 K

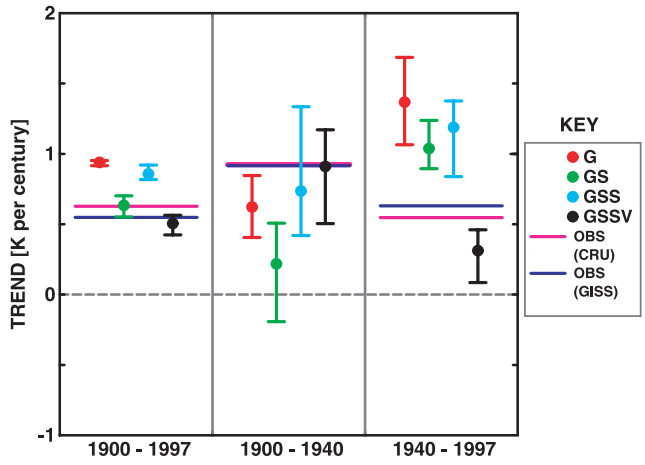

Figure 4. Trends in annually averaged global mean surface air temperature (K $\mathrm{century}^{-1}$) for periods 1900–1997, 1900–1940 and 1940–1997. Each ensemble is represented by a different color: G (red), GS (green), GSS (blue) and GSSV (black). Filled circles indicate trends computed from the ensemble mean time series and horizontal bars indicate the maximum and minimum trends from each ensemble. Longer horizontal bars indicate observed surface temperature trends computed from the CRU (magenta) and GISS (dark blue) data sets. (See text for references.)

(100 yr)$^{-1}$. The larger intraensemble ranges are indicative of the enhanced importance of internal variability as temperature trends are determined over shorter periods [*Stouffer et al.*, 1994].

[28] Among the ensembles, only the GSS and GSSV yield warming trends consistent with the observed estimates for the 1900–1940 period, with the GSSV ensemble mean very close to the observed trend. Both ensembles that neglect the natural forcings are characterized by smaller temperature trends, with none of their members exhibiting warming trends as large as observed. In fact, one of the GS ensemble members underwent a global cooling during this time frame, despite a positive trend in radiative forcing (Figure 4). That internally generated variability could lead to this counterintuitive result illustrates the need for caution in interpreting observed temperature trends, even on multidecadal timescales.

[29] The period from 1940 through 1997 saw the observed global temperature remain relatively steady or decline slightly into the 1970s, then rise sharply over the last 25 years. Integrated over the 1940–1997 period, the result was an observed trend of 0.55 (CRU) to 0.63 (GISS) K (100 yr)$^{-1}$ (Figure 4). The three ensembles that do not include volcanic forcing yield temperature trends that are considerably larger than observed, with no overlap between the ensemble ranges and the observed estimates. In contrast, the GSSV ensemble simulates a much smaller warming trend, underestimating the observed rate of global warming during this period, but with a somewhat smaller discrepancy than the other ensembles.

[30] Considering the degree of consistency between the simulated and observed temperature trends for all three time periods, the GSSV ensemble provides the best overall agreement. This agreement is evident when the GSSV ensemble mean time series of annually averaged, global mean temperature anomalies is compared with CRU and GISS data (Figure 5) for the entire duration of the model runs, beginning in 1865. On the multidecadal timescale, the GSSV simulation generally reproduces the cooling during the late nineteenth century, the warming through 1940, the

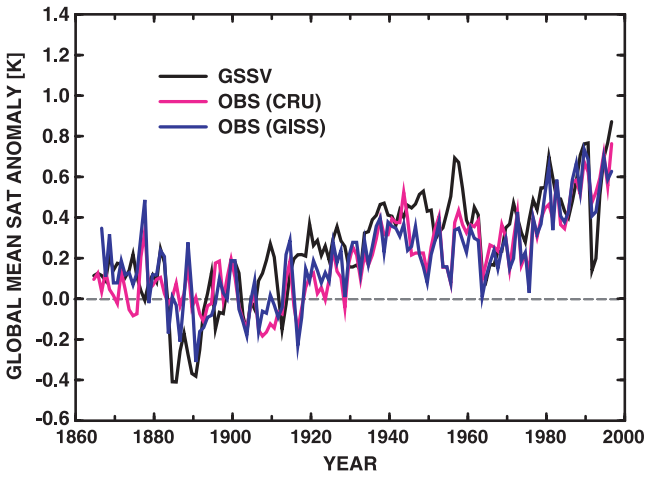

Figure 5. Same as Figure 2 except the GSSV ensemble mean (black) is compared to the observed surface temperature time series of CRU (magenta) and GISS (dark blue).

Table 1. Contributions of Individual Forcings to Overall Warming Trends, as Obtained by Computing the Difference in Trends From Ensembles With and Without That Forcing[a]

	1900–1997	1900–1940	1940–1997
Greenhouse gases	0.94	0.62	1.37
Tropospheric sulfate aerosols	−0.31	−0.40	−0.33
Solar	0.23	0.51	0.15
Volcanic aerosols	−0.35	0.18	−0.88

[a]Units are K (100 yr)$^{-1}$.

period of steady or slowly declining temperature shortly thereafter, and the resumption of warming after 1975. The agreement is not perfect, as might be expected given the presence of substantial unforced interannual variability in both the model and the actual climate system. The evolution of this variability, which arises from the chaotic internal dynamics of the climate system, would not be expected to follow the same course in each of the ensemble members. Similarly, there is no reason to expect the specific evolution of the unforced variability in any of the model simulations to correspond to that of the real climate system.

[31] The design of our experiments does not allow the impact of a single forcing to be directly evaluated, except for the greenhouse gas forcing, which is the only forcing applied in the G ensemble. In order to consider the effects of each forcing individually, their contributions to global temperature change can be assumed to be independent, such that estimates of the sulfate, solar and volcanic forcings can be obtained by subtraction. The assumption of independence cannot be empirically verified or falsified, although there is evidence that supports this assumption [*Haywood et al.*, 1997].

[32] Thus we estimate the sulfate response by subtracting the ensemble mean temperature trend from the G ensemble from the trend from the GS ensemble. An analogous procedure provides estimates of the solar (GSS minus GS) and volcanic (GSSV minus GSS) responses, while the greenhouse gas response can be taken directly from the G ensemble. Trends are computed for each of the periods discussed previously (Table 1).

[33] From this analysis, the simulated century-scale warming trend results from a strongly positive trend from increasing greenhouse gases, a modest solar warming, and moderate coolings from sulfate and volcanic forcing. The similarity of the trends from the GS and GSSV ensembles over this time period can be interpreted as arising from the approximate compensation between the two natural forcings. The solar response is positive because the early century increase in solar irradiance is followed by a period in which irradiance exhibits no multidecadal trend. The volcanic response is negative because of the frequent large eruptions (e.g., Agung, El Chichon, Pinatubo) during the last four decades of the century.

[34] A very different balance between the responses to natural and anthropogenic forcings occurs during the period 1900–1940. Driven by the multidecadal increase in solar irradiance, the solar response of 0.51 K (100 yr)$^{-1}$ is almost as large as the response to greenhouse gases, which is 0.62 K (100 yr)$^{-1}$. The important role of solar forcing is consistent with the work of *Stott et al.* [2001], *Tett et al.* [1999] and *Meehl et al.* [2003], but contrasts with the findings of *Hegerl et al.* [2003], who had difficulty detecting a solar

signal using paleoclimatic reconstructions of Northern Hemisphere temperature. Volcanic forcing also contributes a small warming trend, as the earth emerges from the cooling induced by a period of large explosive eruptions in the late nineteenth and early twentieth centuries. Tropospheric sulfate aerosols contribute a moderate cooling trend.

5. Precipitation Trends

[35] In contrast to the larger number of studies that have compared simulated temperature trends to the observed climate record, relatively few studies have examined precipitation trends in a similar manner. *Hulme et al.* [1998] compared results from the anthropogenically forced runs of the Hadley Centre coupled atmosphere-ocean model HadCM2 with the sensitivity of observed terrestrial precipitation to recent warming. More recently, *Allen and Ingram* [2002] examined changes in precipitation from an ensemble of coupled model runs with the Hadley Centre coupled model HadCM3.

[36] We apply a methodology similar to that of *Hulme et al.* [1998] to the G, GS, GSS and GSSV ensembles in order to better understand the response of global precipitation trends to natural and anthropogenic forcing. Because we wish to compare the simulated time series to observed data throughout the twentieth century, our analysis is limited to land areas, since the use of truly global data sets that incorporate satellite-derived precipitation estimates over oceanic regions is precluded by their brevity. For each integration, a terrestrial precipitation time series is computed by spatially averaging the precipitation over all land points. Four ensemble mean precipitation time series are then computed by averaging over like ensemble members. Each of these sixteen time series (twelve integrations plus four ensemble means), is then expressed as a percentage of the average precipitation for the period 1961–1990. Linear trends are determined by least squares fitting for the same periods used in the temperature trend analysis in section 4.

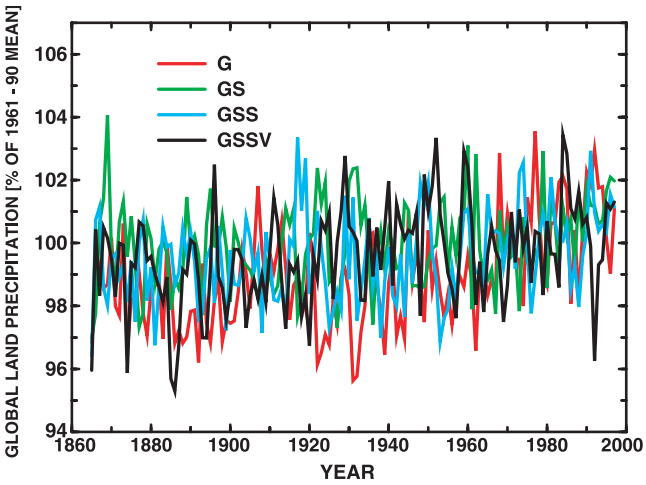

Figure 6. Temporal variation of annually averaged global mean land precipitation, expressed as a percentage of the 1961–1990 average, from the ensemble means of the G (red), GS (green), GSS (blue) and GSSV (black) ensembles.

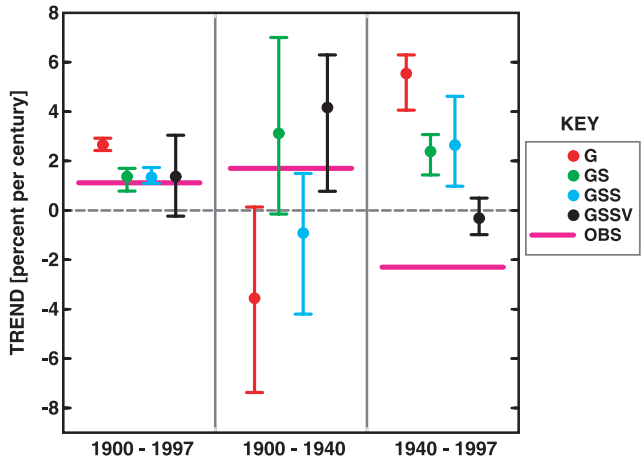

Figure 7. Same as Figure 4 except trends in annually averaged global mean land precipitation (% century^{-1}). Precipitation is expressed as a percentage of the 1961–1990 average (see text for details). Longer horizontal magenta bars indicate the observed trend computed from the *Hulme et al.* [1998] data set.

Observed trends are determined by applying a similar procedure to the terrestrial precipitation data of *Hulme et al.* [1998], employing only those points that correspond to land on the coupled model grid (generally eliminating islands and some coastal points) and have no missing data during the base period 1961–1990. If data are missing for other years, the 1961–1990 average is substituted. The substitution of the climatological mean for missing data could suppress some variability, but this effect is not believed to be important.

[37] Precipitation time series from the twelve individual model integrations (not shown) are characterized by large interannual variability, such that it is difficult to identify even century-scale trends. Ensemble averaging reduces the variability somewhat, and some upward trend is visually evident during the twentieth century in all four ensemble mean time series (Figure 6). Nonetheless, these century-scale precipitation trends are much smaller relative to the high-frequency noise than are the temperature trends discussed in the previous section.

[38] All four sets of forcings yield positive ensemble mean trends for the period 1900–1997 (Figure 7), ranging from 1–3% (100 yr)$^{-1}$. The intraensemble ranges are generally small, except for the GSSV ensemble, which is more than 3% (100 yr)$^{-1}$. Sampling appears to be responsible for the larger range of the GSSV ensemble, as we have found no indication that the unforced variability in the members of this ensemble is larger than in the other three. The trends from the GS, GSS and GSSV ensembles are close to the observed trend of +1.1% (100 yr)$^{-1}$, while the trend from the G ensemble is more than twice as large as observed.

[39] Much more intraensemble variability characterizes the simulated precipitation trends for the shorter periods. For 1900–1940, the intraensemble ranges are from 5–8% (100 yr)$^{-1}$, and the G, GS and GSS ensembles include both positive and negative values. The ensemble mean trends

vary from +4.2% (100 yr)$^{-1}$ in the GSSV ensemble to −3.6% (100 yr)$^{-1}$ in the G ensemble. The observed trend during this period is +1.7% (100 yr)$^{-1}$, and only the ranges of the GS and GSSV ensembles overlap this value. During the 1940–1997 period, most of the individual simulations yield positive trends, with the only negative trends coming from the GSSV ensemble. The intraensemble ranges are smaller than in the first half of the century, with values of roughly 2–5% (100 yr)$^{-1}$. The G ensemble members produce the largest positive trends, with the G ensemble mean trend exceeding 5% (100 yr)$^{-1}$. Smaller positive trends are found in the GS and GSS ensembles. None of the ensemble ranges overlaps the observed trend of −2.3% (100 yr)$^{-1}$, although the GSSV ensemble comes closest.

[40] Several factors may contribute to the observed downward trend in precipitation during the latter half of the twentieth century, including increased frequency of large El Niño events, multidecadal drying of northern tropical Africa, and increased frequency of large tropical volcanic eruptions. In the remainder of this section, we will present the evidence for each of these effects and discuss their expression in the GSSV simulations.

[41] Terrestrial precipitation decreases during El Niño events. *Dai et al.* [1997] found that El Niños are accompanied by a 1–4% decrease in globally averaged land precipitation. *New et al.* [2001] computed a positive correlation (r = 0.62) between the Southern Oscillation Index (SOI) and globally averaged land precipitation, which is consistent with the results of *Dai et al.* [1997] because the SOI is inversely correlated with sea surface temperature (SST) anomalies in the eastern equatorial Pacific. The decrease in terrestrial precipitation is compensated by increased precipitation over oceanic regions, as *Dai and Wigley* [2000] have found global mean precipitation (i.e., land and ocean combined) to be 0.2% above normal during a typical El Niño year. With a number of large El Niño events in the late twentieth century following a period of infrequent events in prior decades, the effects of El Niño may contribute to a decreasing trend in terrestrial precipitation. Relative minima in the observed time series of terrestrial precipitation (Figure 8) occur during the El Niño events of 1982–1983, 1986–1987, 1991–1992 and 1997–1998.

[42] The multidecadal dry spell in northern tropical Africa from the 1970s through the mid-1990s also contributes to the late twentieth century drying. Because the trends in this region contribute substantially to the terrestrial mean, *Dai et al.* [1997] found a mode of variability characterized by a relatively steady upward trend in global land precipitation throughout the twentieth century when they removed northern Africa from their analysis.

[43] The sequence of large tropical volcanic eruptions (i.e., Agung, El Chichón, Pinatubo) that occurred from 1963–1991 may also have reduced terrestrial precipitation. In a modeling study, *Robock and Lin* [1994] noted a decrease in precipitation following volcanic eruptions in a simulation conducted with a climate model developed at the Goddard Institute for Space Studies. In our study, a large downward excursion in terrestrial precipitation follows the Pinatubo eruption in the GSSV ensemble, suggesting that the same response is occurring in the current set of simulations. Observed precipitation also decreases sharply in the aftermath of the Pinatubo eruption, but precipitation variability and the coincidence of this eruption with the 1991–92 El Niño precludes any simple interpretation of this precipitation minimum.

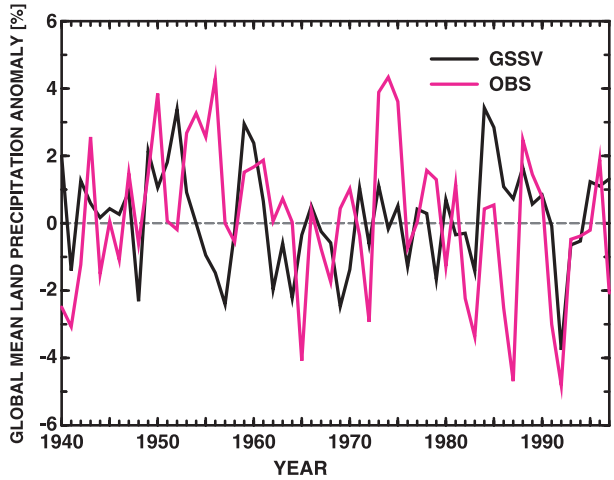

Figure 8. Temporal variation of the GSSV ensemble mean (black) and observed (magenta) monthly global mean land precipitation, expressed as a percentage of the 1961–1990 average. The observed time series is computed from the terrestrial precipitation data set of *Hulme et al.* [1998].

[44] The sequences of El Niño events in each of the individual GSSV simulations would be expected to differ from one another, and none would be expected to coincide with the sequence that occurred in the real climate system. Thus there is no basis for expecting the contribution of multidecadal trends in El Niño frequency in the real climate system to be matched by the GSSV ensemble, even though the coupled model does generate El Niño-like SST variations of similar amplitude to the observed. In addition, a number of hypotheses have been advanced to explain the late twentieth century drying of the Sahel, including mechanisms that are not included in the model, such as human-induced changes in land use and feedbacks involving vegetation. If multidecadal trends in El Niño frequency and Sahel rainfall have contributed substantially to the observed decrease in late twentieth century precipitation, then this drying would likely be underestimated by the GSSV ensemble. There is insufficient evidence to determine if the absence of these mechanisms is responsible for the weakness of the drying in the GSSV ensemble, or if deficiencies in the simulation of mechanisms of precipitation variability and change are the primary cause.

6. Uncertainties in Climate Forcing

[45] Of the forcings used in the climate simulation ensembles described herein, only the greenhouse gas forcings are well-constrained throughout the period of integration. The absence of direct measurements of tropospheric sulfate aerosols, solar irradiance, and stratospheric aerosols from volcanoes requires that reconstructions of their radiative effects be used. In this section, we will discuss some of the uncertainties associated with each of these three forcings, which include uncertainties in magnitude and uncertainties in temporal evolution. Potential climate forcings

agents that have been omitted from the design of the current experiments will also be discussed.

6.1. Tropospheric Sulfate Aerosols

[46] Direct measurements of tropospheric sulfate aerosols do not exist on a global basis for any portion of the time period of the climate model simulations. Such measurements are difficult to make, even with current technology. In developing the spatiotemporal distribution of tropospheric aerosols used in the GS, GSS and GSSV simulations, *Haywood et al.* [1997] used a time history of sulfur emissions and spatial patterns taken from an atmospheric chemistry-transport model. The absence of quantitative global observations, as well as the existence of substantial uncertainties in aerosol microphysics, optical properties and vertical distribution, leads *Ramaswamy et al.* [2001] to estimate an uncertainty of a factor of two for the direct forcing by tropospheric sulfate aerosols. Indirect effects of aerosols have not been included in our experimental design, and such effects could contribute an additional negative forcing, as will be discussed later in this section.

6.2. Solar Irradiance

[47] In addition to the *Lean* [2000] reconstruction, there have been other attempts to estimate the temporal variations in solar irradiance for the period prior to accurate satellite measurements [*Hoyt and Schatten*, 1998; *Solanski and Fligge*, 1998; *Lockwood and Stamper*, 1999]. Each of these reconstructions is somewhat different, but all indicate an increasing trend in solar irradiance during the first half of the twentieth century, and most show little or no multidecadal trend thereafter. Because of these similarities, we would expect that the contribution of solar irradiance to the early twentieth-century warming would have been similar had we used any of these data sets.

[48] Nonetheless, some caution is still required, given the absence of direct measurements. In the IPCC TAR, *Ramaswamy et al.* [2001] described the level of scientific understanding of radiative forcing due to solar irradiance variations as very low, due in part to uncertainties in the relationship between proxies and total solar irradiance and the lack of quantitative measurements going back more than 20 years. More recently, *Lean et al.* [2002] have questioned the reality of low-frequency variability in solar irradiance as reconstructed from geomagnetic proxies. In addition, solar forcing mechanisms other than variations in total solar irradiance have been proposed, as surveyed by *Rind* [2002].

6.3. Stratospheric Aerosols From Volcanoes

[49] As in the case of solar irradiance, direct measurements of volcanic aerosols are confined to the satellite period. Estimates from prior to this time are highly uncertain, and even estimates following recent large eruptions contain considerable uncertainty. *Andronova et al.* [1999] indicate that their estimates of optical depth for the Pinatubo eruption are considerably larger than those of *Sato et al.* [1993]. This discrepancy is also noted by *Hansen et al.* [2002], who suggest that it results from differences in the remote sensing methods used to measure the optical depths. *Hansen et al.* [2002] estimate the uncertainty in volcanic forcing to be approximately 15% for Pinatubo, 20% for El Chichón, 30% for Agung, and 50% for the large eruptions from 1880–1915. The latest IPCC synthesis is more pessimistic than *Hansen et al.* [2002] and estimates that the uncertainty in radiative forcing from eruptions prior to Pinatubo is as much as a factor of two or more [*Ramaswamy et al.*, 2001].

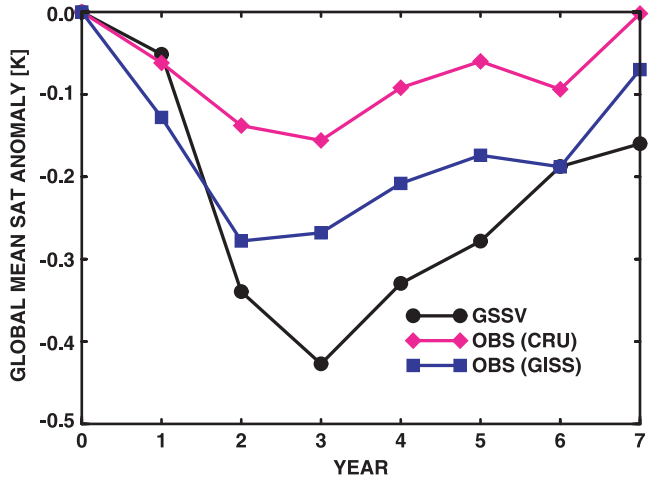

Figure 9. Superposed epoch analysis of post-eruption variations in annually averaged global mean surface air temperature from the GSSV ensemble (black) and the observed CRU (blue) and GISS (red) surface temperature data sets. Five major volcanic eruptions (Krakatau 1883, Santa Maria 1902, Agung 1963, El Chichón 1982 and Pinatubo 1991) are included in this analysis. Temperature anomalies are computed relative to the annual mean temperature in the calendar year during which the eruption occurred, which is defined as year 0.

[50] Because volcanic forcing can be relatively large during short periods following major eruptions, there are a number of opportunities to isolate the climate model's response to this forcing and compare it with observations. A close examination of Figure 5, which compares the GSSV ensemble mean time series of global mean temperature with observations, reveals the possible overestimation of volcanic response in the current set of model simulations. The drop in surface air temperature following the Pinatubo eruption appears almost twice as large in the GSSV ensemble mean as the corresponding change from the CRU or GISS data sets. There is ambiguity to this interpretation, however, since the Pinatubo eruption occurred during a weak but persistent El Niño warm episode, and a similar event would not necessarily be expected to occur in any of the members of the GSSV ensemble at that time. *Santer et al.* [2001] have discussed the difficulties of separating volcanic and El Niño signals.

[51] To further explore the issue of the possible overestimation of volcanic response, a superposed epoch analysis is performed for the periods following five major eruptions. As in *Hansen et al.* [1996], the eruptions used are Krakatau (1883), Santa Maria (1902), Agung (1963), El Chichón (1982) and Pinatubo (1991). For each eruption, the year prior to the eruption is defined as year 0 and the annually averaged global mean temperature for this and subsequent years is plotted as an anomaly relative to year 0. This calculation is performed for the GSSV ensemble mean as well as the CRU and GISS observed temperature data.

[52] The superposed epoch analysis (Figure 9) reveals that the simulated cooling is larger than both of the

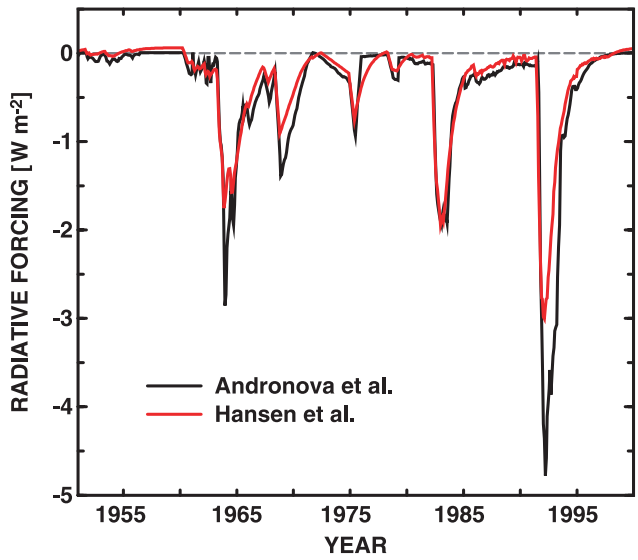

Figure 10. Monthly mean radiative forcing due to volcanic aerosols for the period 1951–1999 from *Andronova et al.* [1999] (black) and *Hansen et al.* [2002] (red).

observational estimates. It is also noteworthy that the cooling in the GISS data set is, at its maximum, more than 60% larger than the corresponding cooling in the CRU data set, indicative of the uncertainty in this type of analysis. *Hansen et al.* [1996] noted that the land bias of the GISS data set may amplify the response to volcanic forcing; they also argue that this may compensate for the poor coverage of temperature changes over the Arctic. Irrespective of which of these two observed data sets more accurately describes the behavior of global temperature following large eruptions, it is clear that the model response is considerably larger than that found in either of the observed data sets.

[53] *Hansen et al.* [2002] recently performed a similar climate simulation experiment using a different set of radiative forcings. They note that the *Andronova et al.* [1999] estimate of the peak Pinatubo volcanic forcing is ~50% larger than their estimate. In fact, the volcanic forcing time series used by Hansen et al. (J. E. Hansen, personal communication, 2002) is of substantially smaller magnitude than that of *Andronova et al.* [1999] for most of the volcanic events in the latter half of the twentieth century (Figure 10).

[54] The simulation by *Soden et al.* [2002] of the climatic aftermath of the 1991 eruption of Mt. Pinatubo is also relevant to an assessment of the uncertainties in volcanic forcing estimates. They used the volcanic aerosol distribution of *Stenchikov et al.* [1998], which is consistent with the volcanic forcing history used in this study, to force a model with many similarities to the one used for the GSSV ensemble. At first glance, the success of *Soden et al.* [2002] in reproducing the global cooling and drying of the atmosphere subsequent to the eruption appears inconsistent with the overestimation of volcanic response in the GSSV ensemble. This inconsistency is only apparent, however, because of an important difference in the atmospheric component of their model. By prescribing the cloud amount, *Soden et al.* [2002] deactivated the cloud feedback in their model. Since a radiative feedback analysis of an earlier version of the model indicated a positive cloud feedback [*Wetherald and Manabe*, 1988], the deactivation of this effect by *Soden et al.* [2002] would decrease the climate sensitivity of their model relative to the model used in this study, and thus yield a smaller thermal response.

[55] In evaluating the differences between the volcanic forcing histories, the excessive cooling of the GSSV ensemble evident in the superposed epoch analysis is consistent with an overestimation of volcanic forcing. However, if one assumes that the *Andronova et al.* [1999] volcanic forcing data are correct, then the successful Pinatubo simulation by *Soden et al.* [2002] would suggest that our model's sensitivity to volcanic forcing could be too large. *Andronova and Schlesinger* [2000] encountered a similar ambiguity in interpreting a mismatch between the cooling in their simple climate model simulations and the observed cooling after the Krakatau and Pinatubo eruptions. A more conclusive assessment is not possible given the available evidence.

6.4. Other Forcings

[56] Temporal variations in a number of climate forcing agents are not included in any of our simulations, including ozone (stratospheric and tropospheric), fossil fuel carbon (black and organic), biomass burning, mineral dust, indirect effects of sulfate aerosols, and land use changes. On the basis of the evaluation made in IPCC TAR by *Ramaswamy et al.* [2001], the level of scientific understanding for most of these forcing agents is very low. The exception is ozone, for which the level of scientific understanding is described as moderate. For most of these individual forcing agents, the global and annual mean radiative forcing from 1750 to the present is relatively small, with best-guess magnitudes of 0.35 W m^{-2} or less. For mineral dust and the indirect effects of tropospheric sulfate aerosols, no best-guess value is given by *Ramaswamy et al.* [2001]. In the case of mineral dust, even the sign of the forcing is uncertain, whereas the indirect sulfate forcing is believed to be negative, but with a range of uncertainty from 0 to -2 W m^{-2}.

[57] Aside from the potentially large indirect sulfate forcing, it appears unlikely that the forcing agents we have neglected represent an important radiative influence on the global near-surface climate, when taken collectively. Some cancellation occurs between positive (tropospheric ozone, fossil fuel black carbon) and negative (stratospheric ozone, fossil fuel organic carbon, biomass burning, land use) forcings. Given the uncertainties associated with each of these forcings, we cannot discount the possibility that a climatically important net forcing could result from these neglected agents. Nor can we exclude the possibility that the simulated temperature and precipitation trends might be altered, at least quantitatively, by the inclusion of the neglected forcings.

7. Discussion

[58] On the basis of the ensemble simulations conducted in this study, observed global mean temperature trends during the twentieth century are best simulated by including both anthropogenic and natural forcings. The GSSV ensemble yields the best agreement with observed temperature

trends for all three periods considered (1900–1997, 1900–1940, 1940–1997). Although good agreement with observed century-scale trends is possible even when natural forcings are neglected, as in the GS ensemble, the early century warming trend is underestimated and the late-century trend is overestimated. The addition of natural forcings bring the trends during these shorter periods into better agreement with the observed record, with solar forcing the key addition during the 1900–1940 period and volcanic forcing the more important contributor from 1940–1997.

[59] For precipitation trends over land, the GSSV ensemble again yields the best agreement with observations when considering all of the periods that were examined. The range of the GSSV ensemble is the only one that overlaps the observed trend for the 1900–1997 and 1900–1940 periods, and the GSSV ensemble comes closest to simulating the reduction of land precipitation during the 1940–1997 period. As with temperature, the discrepancy between simulated and observed precipitation trends is larger when natural forcings are neglected, as in the GS ensemble.

[60] Previous work by *Levitus et al.* [2001], in which the observed trend in ocean heat content for the period 1955–1996 was compared to the trends simulated in the GS and GSSV ensembles, also finds better agreement when natural forcings are included. The intervals of negative radiative forcing caused by the Agung, El Chichón and Pinatubo eruptions temporarily interrupt the uptake of heat by the ocean, causing the heat uptake in the GSSV ensemble to be 40% smaller than that in the GS ensemble.

[61] In synthesizing results on the detection and attribution of climate change for IPCC TAR, *Mitchell et al.* [2001] concluded that including the effects of solar and volcanic forcings "...brings the low-frequency variability simulated by models closer to that deduced from palaeo-reconstructions." Our results regarding low-frequency climate variations during the twentieth century are consistent with this conclusion. The results of this study, as well as those of *Levitus et al.* [2001], indicate that twentieth-century trends in temperature, precipitation and ocean heat content are simulated more realistically by our climate model when natural forcings due to volcanoes and solar irradiance variations are included. The importance of natural forcings in our experiments is consistent with the finding by *Meehl et al.* [2003] that solar forcing is an important factor in early twentieth-century warming. Our results are also consistent with those derived from simpler models over longer time periods [*Crowley*, 2000], and results from more formal detection-attribution studies based on output from other coupled atmosphere-ocean models [*Tett et al.*, 1999; *Stott et al.*, 2001].

[62] The role of natural forcing in early twentieth century temperature trends is one of the keys to understanding an apparent paradox regarding global warming. Those skeptical of the importance of anthropogenic effects on climate often cite the relatively rapid warming during the period, a time when greenhouse gases were growing relatively slowly, as evidence that greenhouse gas levels and global temperatures are only weakly connected [e.g., *Kerr*, 2000]. The results from the set of ensemble simulations described in this study provide a solution to this paradox; the early century warming was augmented by solar and volcanic forcing. Similarly, the more rapid growth of greenhouse gas concentrations during the latter portion of the twentieth century has been partially offset by stratospheric injections of volcanic aerosols from the eruptions of the past several decades. Thus the contribution of natural climate forcings to observed temperature trends supports, rather than contradicts, the climatic importance of changes in atmospheric composition during the twentieth century.

[63] Unforced variability internal to the coupled atmosphere-ocean system also plays a prominent role in determining multidecadal trends in temperature and precipitation. Both for global mean temperature and terrestrial precipitation, the intraensemble range of the simulated trends is substantial for the periods of four to six decades in length that we examined. As an example, in one member of the GS ensemble a negative temperature trend was simulated for the period 1900–1940 despite a net positive radiative forcing. In the case of precipitation, the intraensemble ranges are comparable in magnitude to the trends. Consequently, substantial uncertainty is introduced in the interpretation of observed precipitation trends, since there is only a single realization of the actual climate history. Even for global mean temperature, timescales approaching a century are required for intraensemble ranges to become substantially smaller than the simulated trends, despite the small sample size (i.e., ensemble members) available for determining the intraensemble ranges. Thus the possibility that unforced variability could also have contributed substantially to the warming of the early twentieth century, as suggested by *Delworth and Knutson* [2000], remains viable.

[64] The results presented herein add to a growing body of climate modeling studies that suggest that a substantial fraction of the low-frequency variation in global climate during the twentieth century is radiatively forced, and that natural forcing agents have been important contributors. Using the Hadley Centre coupled atmosphere-ocean model HadCM2, *Tett et al.* [1999] concluded that while anthropogenic forcing is the most likely source of late twentieth century warming, solar forcing may have contributed to early century warming. *Stott et al.* [2001] used optimal detection techniques to attribute some of the early twentieth century warming to volcanic and, possibly, solar forcing, with anthropogenic forcing contributing throughout the century. Using a later version of the Hadley Centre coupled model (HadCM3), *Stott et al.* [2000] found that both anthropogenic and natural factors have contributed to twentieth century temperature changes, with the combination of these factors responsible for more than 80% of multidecadal variations in global mean temperature. *Meehl et al.* [2003] also found that a combination of natural and anthropogenic forcing contributed to the simulation of early century warming in the Parallel Climate Model of the National Center for Atmospheric Research.

[65] Finally, retrospective climate simulations of the kind presented herein should remain an essential element of our future climate modeling activities. As discussed in section 6, large uncertainties exist in current estimates of the magnitude and temporal evolution of natural and anthropogenic forcing agents. As better methods are developed to quantify and reconstruct these forcings, experiments such as these should be repeated to determine if the conclusions would be altered. In addition, paleoclimatic

methods offer great promise in extending the instrumental climate record backward in time [*Jones et al.*, 1998; *Mann et al.*, 1999; *Briffa*, 2000; *Esper et al.*, 2002]. As such records are developed, longer retrospective simulations will also be of value. The challenge will be to develop and use climate models that strike the correct balance between comprehensiveness, which adds to their computational cost, and the ability to make multicentury ensemble simulations, which requires computational efficiency.

8. Summary

[66] The relative importance of natural and anthropogenic forcings to twentieth-century climate trends is investigated by running four sets of ensemble integrations of a global coupled atmosphere-ocean model for the period 1865–1997. Each ensemble consists of three integrations initialized from different points in a long-running GFDL R30 coupled model control simulation. The first ensemble includes time-varying forcing from greenhouse gases only. Forcings from anthropogenic sulfate aerosols, solar variability, and volcanic aerosols in the stratosphere are added progressively in the remaining three ensembles, such that the fourth uses all four of these forcings. Simulated trends in global mean temperature, terrestrial precipitation and ocean heat content are compared with observations. We find that (1) the addition of the natural forcings (solar and volcanic) improves the simulation of global multidecadal trends in temperature, precipitation, and ocean heat content, (2) solar and volcanic forcings are important contributors to early twentieth century warming, (3) volcanic forcing reduces the warming simulated for the late twentieth century, and (4) the ensemble of experiments with all four forcings yields a time-varying global mean surface air temperature response that closely resembles that observed during all portions of the twentieth century.

[67] Although there is some discrepancy between simulated and observed trends in temperature and precipitation during the latter half of the century, possibly due to model sensitivity or erroneous or neglected forcings, these results suggest that current climate models are capable of simulating many of the globally averaged, multidecadal variations in near-surface climate as a response to radiative forcing.

[68] **Acknowledgments.** We are grateful to G. Hegerl, H. Levy II, B. J. Soden, V. Ramaswamy and two anonymous reviewers for their comments on previous drafts of this paper. We are also indebted to S. Manabe for his leadership and vision, which contributed to the development of the coupled atmosphere-ocean model used in this study.

References

Allen, M. R., and W. J. Ingram, Constraints on future changes in climate and the hydrologic cycle, *Nature*, *419*, 224–232, 2002.

Andronova, N., and M. E. Schlesinger, Causes of global temperature changes during the 19th and 20th centuries, *Geophys. Res. Lett.*, *27*, 2137–2140, 2000.

Andronova, N. G., E. V. Rozanov, F. Yang, M. E. Schlesinger, and G. L. Stenchikov, Radiative forcing by volcanic aerosols from 1850 to 1994, *J. Geophys. Res.*, *104*, 16,807–16,826, 1999.

Briffa, K. R., Annual climate variability in the Holocene: Interpreting the message of ancient trees, *Quat. Sci. Rev.*, *19*, 87–105, 2000.

Crowley, T. J., Causes of climate change over the past 1000 years, *Science*, *289*, 270–277, 2000.

Cubasch, U., et al., Projections of future climate change, in *Climate Change 2001: The Scientific Basis*, edited by J. T. Houghton et al., pp. 525–582, Cambridge Univ. Press, New York, 2001.

Dai, A., and T. M. L. Wigley, Global patterns of ENSO-induced precipitation, *Geophys. Res. Lett.*, *27*, 1283–1286, 2000.

Dai, A., I. Y. Fung, and A. D. DelGenio, Surface observed global land precipitation variations during 1900–1988, *J. Clim.*, *10*, 2943–2962, 1997.

Delworth, T. L., and T. R. Knutson, Simulation of early 20th century global warming, *Science*, *287*, 2246–2250, 2000.

Delworth, T. L., A. J. Broccoli, K. W. Dixon, T. R. Knutson, P. J. Kushner, M. J. Spelman, R. J. Stouffer, and R. T. Wetherald, Simulation of climate variability and change by the GFDL R30 coupled climate model, *Clim. Dyn.*, *9*, 555–574, 2002.

Dixon, K. W., and J. R. Lanzante, Global mean surface air temperature and North Atlantic overturning in a suite of coupled GCM climate change experiments, *Geophys. Res. Lett.*, *26*, 1885–1888, 1999.

Esper, J., E. R. Cook, and F. H. Schweingruber, Low-frequency signals in long tree-ring chronologies for reconstructing past temperature variability, *Science*, *295*, 2250–2253, 2002.

Haigh, J. D., The impact of solar variability on climate, *Science*, *272*, 981–984, 1996.

Hansen, J. E., D. Johnson, A. Lacis, S. Lebedeff, P. Lee, D. Rind, and G. Russell, Climate impact of increasing carbon dioxide, *Science*, *213*, 957–966, 1981.

Hansen, J. E., et al., A Pinatubo climate modeling investigation, in *The Mount Pinatubo Eruption: Effects on the Atmosphere and Climate*, *NATO ASI Series Vol. I*, vol. 42, edited by G. Fiocco, D. Fua, and G. Visconti, pp. 233–272, Springer-Verlag, New York, 1996.

Hansen, J., R. Ruedy, J. Glascoe, and M. Sato, GISS analysis of surface temperature change, *J. Geophys. Res.*, *104*, 30,997–31,022, 1999.

Hansen, J., et al., Climate forcings in Goddard Institute for Space Studies SI2000 simulations, *J. Geophys. Res*, *107*(D18), 4347, doi:10.1029/2001JD001143, 2002.

Hasselmann, K., R. Sausen, E. Maier-Reimer, and R. Voss, On the cold start problem in transient simulations with coupled ocean-atmosphere models, *Clim. Dyn.*, *9*, 53–61, 1993.

Haywood, J. M., R. J. Stouffer, R. T. Wetherald, S. Manabe, and V. Ramaswamy, Transient response of a coupled model to estimated changes in greenhouse gas and sulfate concentrations, *Geophys. Res. Lett.*, *24*, 1335–1338, 1997.

Hegerl, G. C., T. J. Crowley, S. K. Baum, K.-Y. Kim, and W. T. Hyde, Detection of volcanic, solar and greenhouse gas signals in paleo-reconstructions of Northern Hemispheric temperature, *Geophys. Res. Lett.*, *30*(5), 1242, doi:10.1029/2002GL016635, 2003.

Houghton, J. T., Y. Ding, D. J. Griggs, M. Noguer, P. J. van der Linden, X. Dai, K. Maskell, and C. A. Johnson (Eds.), *Climate Change 2001: The Scientific Basis*, Cambridge Univ. Press, New York, 2001.

Hoyt, D. V., and K. H. Schatten, Group sunspot numbers: A new solar activity reconstruction, *Sol. Phys.*, *181*, 491–512, 1998.

Hulme, M., T. J. Osborn, and T. C. Johns, Precipitation sensitivity to global warming: Comparison of observations with HadCM2 simulations, *Geophys. Res. Lett.*, *25*, 3379–3382, 1998.

Jones, P. D., K. R. Briffa, T. P. Barnett, and S. F. B. Tett, High-resolution palaeoclimatic records for the last millennium: Interpretation, integration and comparison with general circulation model control run temperatures, *The Holocene*, *8*, 455–471, 1998.

Jones, P. D., M. New, D. E. Parker, S. Martin, and I. G. Rigor, Surface air temperature and its changes over the past 150 years, *Rev. Geophys.*, *37*, 173–199, 1999.

Kerr, R. A., North Atlantic climate pacemaker for the centuries, *Science*, *288*, 1984–1985, 2000.

Langner, I., and H. Rodhe, A global three-dimensional model of the tropospheric sulfur cycle, *J. Atmos. Chem.*, *13*, 225–263, 1991.

Lean, J., Evolution of the sun's spectral irradiance since the Maunder Minimum, *Geophys. Res. Lett.*, *27*, 2425–2428, 2000.

Lean, J. L., Y.-M. Wang, and N. R. Sheeley Jr., The effect of increasing solar activity on the Sun's total and open magnetic flux during multiple cycles: Implications for solar forcing of climate, *Geophys. Res. Lett.*, *29*(24), 2224, doi:10.1029/2002GL015880, 2002.

Leggett, J., W. J. Pepper, and R. J. Swart, Emissions scenarios for the IPCC: An update, in *Climate Change 1992: The Supplementary Report to the IPCC Scientific Assessment*, edited by J. T. Houghton, B. A. Callander, and S. K. Varney, pp. 69–95, Cambridge Univ. Press, New York, 1992.

Levitus, S., J. I. Antonov, J. Wang, T. L. Delworth, K. W. Dixon, and A. J. Broccoli, Anthropogenic warming of Earth's climate system, *Science*, *292*, 267–270, 2001.

Lockwood, M., and R. Stamper, Long-term drift of the coronal source magnetic flux and the total solar irradiance, *Geophys. Res. Lett.*, *26*, 2461–2464, 1999.

Manabe, S., R. J. Stouffer, M. J. Spelman, and K. Bryan, Transient responses of a coupled ocean-atmosphere model to gradual changes of atmospheric CO_2: Part I. Annual mean response, *J. Clim.*, *4*, 785–818, 1991.

Mann, M. E., R. S. Bradley, and M. K. Hughes, Northern hemisphere temperatures during the past millennium: Inferences, uncertainties, and limitations, *Geophys. Res. Lett.*, *26*, 759–762, 1999.

Meehl, G. A., W. M. Washington, T. M. L. Wigley, J. M. Arblaster, and A. Dai, Solar and greenhouse forcing and climate response in the twentieth century, *J. Clim.*, *16*, 426–444, 2003.

Mitchell, J. F. B., and T. C. Johns, On modification of global warming by sulfate aerosols, *J. Clim.*, *10*, 245–267, 1997.

Mitchell, J. F. B., T. C. Johns, J. M. Gregory, and S. F. B. Tett, Climate response to increasing levels of greenhouse gases and sulphate aerosols, *Nature*, *376*, 501–504, 1995.

Mitchell, J. F. B., et al., Detection of climate change and attribution of causes, in *Climate Change 2001: The Scientific Basis.*, edited by J. T. Houghton et al., pp. 695–738, Cambridge Univ. Press, New York, 2001.

New, M., M. Todd, M. Hulme, and P. Jones, Precipitation measurements and trends in the twentieth century, *Int. J. Climatol.*, *21*, 1899–1922, 2001.

Pacanowski, R., K. Dixon, and A. Rosati, The GFDL modular ocean model users guide version 1, *GFDL Ocean Group Tech. Rep. 2*, NOAA/Geophys. Fluid Dyn. Lab., Princeton, N.J., 1991.

Ramaswamy, et al., Radiative forcing of climate change, in *Climate Change 2001: The Scientific Basis*, edited by J. T. Houghton et al., pp. 349–416, Cambridge Univ. Press, New York, 2001.

Rind, D., The sun's role in climate variations, *Science*, *296*, 673–677, 2002.

Robock, A., Volcanic eruptions and climate, *Rev. Geophys.*, *38*, 191–219, 2000.

Robock, A., and Y. Liu, The volcanic signal in Goddard Institute for Space Studies three-dimensional model simulations, *J. Clim.*, *7*, 44–55, 1994.

Santer, B. D., T. M. L. Wigley, C. Doutriaux, J. S. Boyle, J. E. Hansen, P. D. Jones, G. A. Meehl, E. Roeckner, S. Sengupta, and K. E. Taylor, Accounting for the effects of volcanoes and ENSO in comparisons of modeled and observed temperature trends, *J. Geophys. Res.*, *106*, 28,033–28,059, 2001.

Sato, M., J. E. Hansen, M. P. McCormick, and J. P. Pollack, Stratospheric aerosol optical depths, 1850–1990, *J. Geophys. Res.*, *98*, 22,987–22,994, 1993.

Shindell, D., D. Rind, N. Balachandran, J. Lean, and P. Lonergan, Solar cycle variability, ozone, and climate, *Science*, *284*, 305–308, 1999.

Shine, K. P., R. G. Derwent, D. J. Wuebbles, and J.-J. Morcrette, Radiative forcing of climate, in *Climate Change 1990: The IPCC Scientific Assessment*, edited by J. T. Houghton, G. J. Jenkins, and J. J. Ephraums, pp. 41–68, Cambridge Univ. Press, New York, 1990.

Soden, B. J., R. T. Wetherald, G. L. Stenchikov, and A. Robock, Global cooling after the eruption of Mount Pinatubo: A test of climate feedback by water vapor, *Science*, *296*, 727–730, 2002.

Solanski, S. K., and M. Fligge, Solar irradiance since 1874 revisited, *Geophys. Res. Lett.*, *25*, 341–344, 1998.

Stenchikov, G. L., I. Kirchner, A. Robock, H.-F. Graf, J. C. Antuña, R. G. Grainger, A. Lambert, and L. Thomason, Radiative forcing from the 1991 Mount Pinatubo volcanic eruption, *J. Geophys. Res.*, *103*, 13,837–13,857, 1998.

Stott, P. A., S. F. B. Tett, G. S. Jones, M. R. Allen, J. F. B. Mitchell, and G. J. Jenkins, External control of 20th century temperature by natural and anthropogenic forcings, *Science*, *290*, 2133–2137, 2000.

Stott, P. A., S. F. B. Tett, G. S. Jones, M. R. Allen, W. J. Ingram, and J. F. B. Mitchell, Attribution of twentieth century temperature change to natural and anthropogenic causes, *Clim. Dyn.*, *17*, 1–21, 2001.

Stouffer, R. J., and K. W. Dixon, Initialization of coupled models for use in climate studies: A review, in *Research Activities in Atmospheric and Oceanic Modelling*, *Rep. 27*, *WMO/TD-No. 865*, pp. I.1–I.8, World Meteorol. Org., Geneva, Switzerland, 1998.

Stouffer, R. J., S. Manabe, and K. Y. Vinnikov, Model assessment of the role of natural variability in recent global warming, *Nature*, *367*, 634–636, 1994.

Tett, S. F. B., P. A. Stott, M. R. Allen, W. J. Ingram, and J. F. B. Mitchell, Causes of twentieth-century temperature change near the Earth's surface, *Nature*, *399*, 569–572, 1999.

Wetherald, R. T., and S. Manabe, Cloud feedback processes in a general circulation model, *J. Atmos. Sci.*, *45*, 1397–1415, 1988.

A. J. Broccoli, Department of Environmental Sciences, Rutgers University, 14 College Farm Road, New Brunswick, NJ 08901, USA. (broccoli@envsci.rutgers.edu)

T. L. Delworth, K. W. Dixon, T. R. Knutson, and R. J. Stouffer, NOAA/Geophysical Fluid Dynamics Laboratory, Princeton University, Princeton, NJ 08542, USA.

F. Zeng, RSIS, Princeton, NJ 08540, USA.